



ELSEVIER

Computer Physics Communications 112 (1998) 91–101

Computer Physics
Communications

Computation of photoelectron and Auger-electron diffraction III. Evaluation of angle-resolved intensities PAD3

X. Chen, G.R. Harp¹, Y. Ueda, D.K. Saldin²

Department of Physics and Laboratory for Surface Studies, University of Wisconsin-Milwaukee, P.O. Box 413, Milwaukee, WI 53201, USA

Received 10 December 1996; revised 1 December 1997

Abstract

In this paper, we describe the third part of a suite of computer programs for the computation of Auger- and photoelectron diffraction intensities, using the so-called concentric shell algorithm (CSA). The function of the present program is to calculate the diffraction intensities capable of being measured in a variety of different experimental configurations. The present program takes as its input the cluster transmission matrix calculated in the second part of this sequence of programs, as well as the spherical wave amplitudes of the atomic photoemission process, and other input specifying the type of experiment. The output of this program is a file containing the diffraction intensities in a form for direct comparison with experimental results. © 1998 Elsevier Science B.V.

PACS: 61.14.Qp; 61.14.Dc; 68.35.Bs

Keywords: Angle resolved; Core-level; Photoelectron; Auger; Electron diffraction; Surface structure; Multiple scattering; Electron spectroscopy

PROGRAM SUMMARY

Title of program: PAD3

it is operable: DEC-alpha and Silicon Graphics workstations, and CRAY and NEC supercomputers

Catalogue identifier: ADIB

Operating systems under which the program has been tested: UNIX

Program Summary URL:

Program language used: FORTRAN-77

<http://www.cpc.cs.qub.ac.uk/cpc/summaries/ADIB>

Memory required to execute with typical data: 1.7 mega-words

Program obtainable from: CPC Program Library, Queen's University of Belfast, N. Ireland

No. of bits in a word: 64

Licensing provisions: none

No. of processors used: 1

Computer for which the program is designed and others on which

Has the code been vectorised or parallelized? No

¹ Permanent address: Department of Physics and Astronomy, Ohio University, Athens, OH 45701.

² Corresponding author; e-mail: dksaldin@csd.uwm.edu.

No. of bytes in distributed program, including test data, etc.:
33917

Distribution format: uuencoded compressed tar file

Keywords: Angle resolved, core-level, photoelectron, Auger, electron diffraction, surface structure, multiple scattering, electron spectroscopy

Nature of physical problem

Multiple scattering cluster calculation of angle-resolved core-level photoelectron diffraction and Auger-electron diffraction via a concentric-shell algorithm (CSA).

Restrictions on the complexity of the problem

For photoelectron diffraction, only s , p , d , and f core-level emission are allowed in the present code.

Typical running time

For the test run, the PAD3 program took 23 seconds to execute on a Silicon Graphics Indigo² computer equipped with an R10000 processor.

Unusual features of the program

None.

LONG WRITE-UP

1. Introduction

X-ray photoelectron diffraction (PD) and Auger-electron diffraction (AD) are useful tools for the investigation of surface crystallography. Recent work has shown that the angular-momentum character of an emitted atomic core electron is an important determinant of the form of Auger- and photoelectron diffraction patterns [1], especially for low energies of the emitted electron. The diffraction pattern will also be sensitive to the details of the experimental geometry. In contrast, for higher electron kinetic energies, atomic scattering factors are very forward peaked, and the resulting diffraction pattern will be much less sensitive to the character of the initially photoemitted wave.

In this paper III of our set of papers, we will describe, in some detail, some common experimental configurations, and will show how the present program may be used to simulate the diffraction intensities expected in each case. Both PD and AD will be considered.

2. Photoemission: transforming from the laboratory frame to the frame of reference of the sample

In paper I [4] of this set, we described the calculation by the PAD1 program of the amplitude, $B_{nL_c,L}^{(0)'}$, of the spherical wave representing the electron emitted from an atomic core state of quantum numbers nL_c into an outgoing state of angular momentum L . This primed amplitude refers to the *laboratory* frame of reference, \mathbf{a}' , the z -axis of which is parallel to the magnetic vector potential \mathbf{A} . These amplitudes are read in by the present program, PAD3. In order to calculate the wavefunction after the electron's scattering by the surrounding cluster of atoms, it is necessary first to transform these amplitudes into those, $B_{nL_c,L}^{(0)}$, defined instead with respect to a frame of reference $\mathbf{a} = (x, y, z)$ fixed relative to the sample. This may be done with the aid of the rotation matrix elements [3],

$$D_{m',m}^{(l)}(\mathbf{a}, \mathbf{a}') = e^{im'\gamma + im\alpha} d_{m',m}^{(l)}(\beta), \quad (1)$$

where α , β and γ are the Euler angles relating the two frames of reference. The functions $d_{m',m}^{(l)}(\beta)$ are determined by the expression

$$d_{m',m}^{(l)}(\beta) = \left(\frac{(l+m')!(l-m')!}{(l+m)!(l-m)!} \right)^{1/2} (\cos(\beta/2))^{m'+m} (\sin(\beta/2))^{m'-m} P_{l-m'}^{(m'-m, m'+m)}(\cos \beta), \quad (2)$$

where the functions $P_l^{m,n}(x)$ are the Jacobi polynomials. The quantities $d_{m',m}^{(l)}(\beta)$ obey the symmetry relations

$$d_{m',m}^{(l)}(\beta) = d_{-m,-m'}^{(l)}(\beta) \quad (3)$$

and

$$d_{m',m}^{(l)}(\beta) = (-)^{m+m'} d_{m,m'}^{(l)}(\beta) \quad (4)$$

and can be calculated for $m' \geq 0$ and $|m| \leq m'$ by using the following recurrence relations:

$$\begin{aligned} b_{l+1,m} b_{l+1,m'} d_{m',m}^{(l+1)}(\beta) &= (2l+1)[(l+1) \cos \beta - mm'/l] d_{m',m}^{(l)}(\beta) \dots \\ &\quad - ((l+1)/l) b_{l,m} b_{l,m'} d_{m',m}^{(l-1)}(\beta), \end{aligned} \quad (5)$$

where $b_{l,m} = \sqrt{l^2 - m^2}$, and the initial values are

$$d_{m',m}^{(m')}(\beta) = 2^{-m'} \left(\frac{(2m')!}{(m'+m)!(m'-m)!} \right)^{1/2} (\cos(\beta/2))^{m'+m} (\sin(\beta/2))^{m'-m} \quad (6)$$

and

$$d_{m',m}^{(m'+1)}(\beta) = \left(\frac{(2m'+1)}{(m'+m+1)(m'-m+1)} \right)^{1/2} ((m'+1) \cos \beta - m) d_{m',m}^{(m')}(\beta). \quad (7)$$

Combining above equations, one may write

$$D_{m'm}^{(l)}(\theta_\varepsilon, \phi_\varepsilon) = e^{-im\phi} \left(\frac{(l+m')!(l-m')!}{(l+m)!(l-m)!} \right)^{1/2} \frac{(\cos(\theta_\varepsilon/2))^{m'+m}}{(\sin(\theta_\varepsilon/2))^{m'-m}} P_{l-m'}^{(m'-m, m'+m)}(\cos \theta_\varepsilon), \quad (8)$$

where the Euler angles α , β and γ are set equal to θ_ε , ϕ_ε and zero, respectively. The angles θ_ε and ϕ_ε are the polar and azimuthal angles of the magnetic vector potential \mathbf{A} (which is also parallel to the electric-field vector \mathbf{e} of the electromagnetic wave) relative to the sample's frame of reference.

These matrix elements allow the calculation of the spherical wave amplitudes $B_{nL_c,L}^{(0)}$ in the sample's reference frame from those $B_{nL_c,L}^{(0)'} \infty$ in the laboratory frame by means of the linear relation

$$B_{nL_c,lm}^{(0)} = \sum_{m'} D_{m'm}^{(l)}(\theta_\varepsilon, \phi_\varepsilon) B_{nL_c,l'm'}^{(0)'}. \quad (9)$$

This relation enables the computation of angle-resolved photoemission intensities for arbitrary directions of the X-ray polarization vector relative to a sample.

3. Angle-resolved photoelectron diffraction intensities

The spherical wave amplitudes $B_{nL_c,L}^{(0)}$, calculated as described above, are then used to evaluate the measurable far-field intensity distribution after the scattering of the emitted electron by the cluster of atoms surrounding the emitter. The angle-resolved photoelectron intensity distribution may be evaluated from [2]

$$I_{PD}(\hat{\mathbf{k}}) = \sum_{L_c} \left| \sum_L B_{nL_c,L}^{(0)} \sum_{L'} S_{LL'}(-i)^{l'} Y_{L'}(\hat{\mathbf{k}}) \right|^2 \exp\{-z/\lambda \cos(\theta)\}, \quad (10)$$

where λ is the inelastic scattering length of the electron, z the depth of the emitter below the surface of the sample, and θ the angle between the detected wavevector $\hat{\mathbf{k}}$ and the surface normal. The above expression implies that the emitted angular momentum components L arising from the same core state, characterized by L_c , are mutually coherent, while those from different core states are assumed to be mutually incoherent.

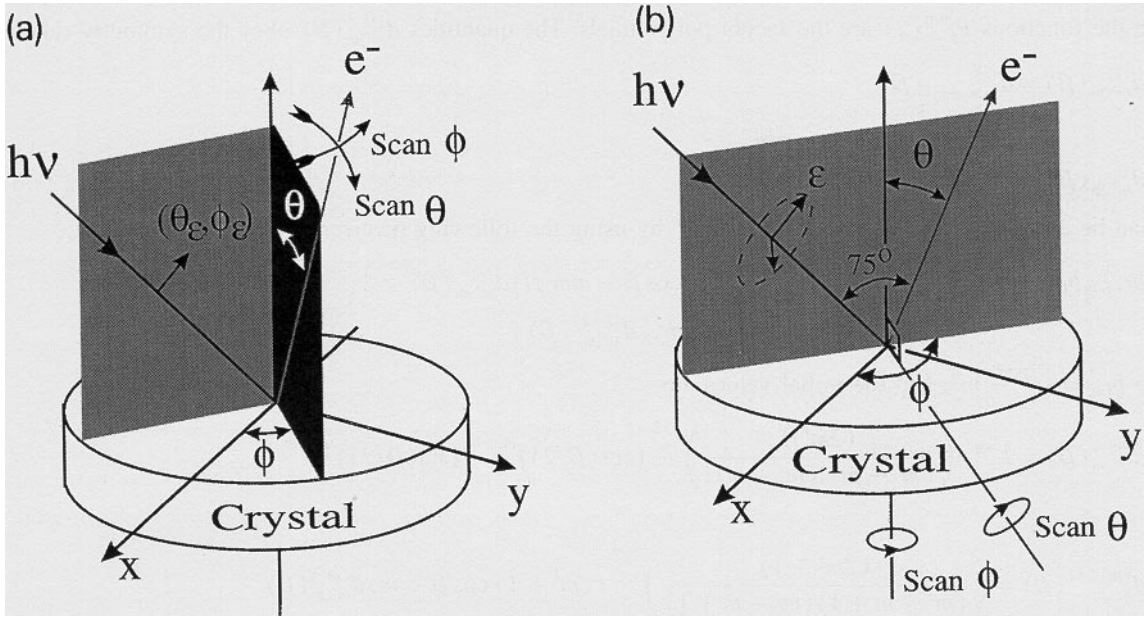


Fig. 1. (a) Schematic diagram of the experimental geometry PD1. The sample and X-ray beam are fixed, with the sample normal in the plane, defined as the X-ray plane, containing incident the X-ray beam and the X-ray polarization vector. Angle-resolved PD intensities are measured by moving the detector to scan both the θ and ϕ angles.

(b) Schematic diagram of the experimental geometry PD2. The X-ray beam and detector are fixed, with the incident X-ray beam, electron exit direction, and sample normal in the same plane, and with an angle of 75° between electron exit direction and that of the incident X-ray beam. Angle-resolved PD intensities are measured by rotating the sample to scan both the ϕ and θ detection angles.

(c) Schematic diagram of the experimental geometry of PD3. The X-ray beam is fixed, with the sample normal and the electron exit direction in the X-ray plane (as defined in (a)). Angle-resolved PD intensities are measured by moving the detector to scan θ and by rotating the sample to scan ϕ .

(d) Schematic diagram of the experimental geometry PD4. The X-ray beam and detector are fixed, with the electron exit direction being in the X-ray plane, which is tilted by an angle θ off the sample normal. Angle-resolved PD intensities are measured by rotating the sample to vary θ and ϕ .

4. Angle-resolved Auger electron diffraction intensities

In the case of Auger emission, we assume that the emitted electron's angular momentum channels L are mutually incoherent. This implies that the angular distribution of an Auger electron diffraction pattern may be evaluated from [2],

$$I_{AD}(\hat{\mathbf{k}}) = \sum_L \left| B_{\text{Aug},L}^{(0)} \sum_{L'} S_{LL'}(-i)^l Y_{L'}(\hat{\mathbf{k}}) \right|^2 \exp\{-z/\lambda \cos(\theta)\} \quad (11)$$

where the amplitudes $B_{\text{Aug},L}^{(0)}$ are related to the matrix elements for Auger transitions, and read in from the data file `cluster.out` created by the PAD1 program. Isotropic Auger emission may be ensured by requiring that the amplitudes of the emitted waves of different magnetic quantum numbers m , corresponding to a particular azimuthal quantum number l , are taken to be equal, i.e. that

$$B_{\text{Aug},lm}^{(0)} \equiv B_{\text{Aug},l}^{(0)}. \quad (12)$$

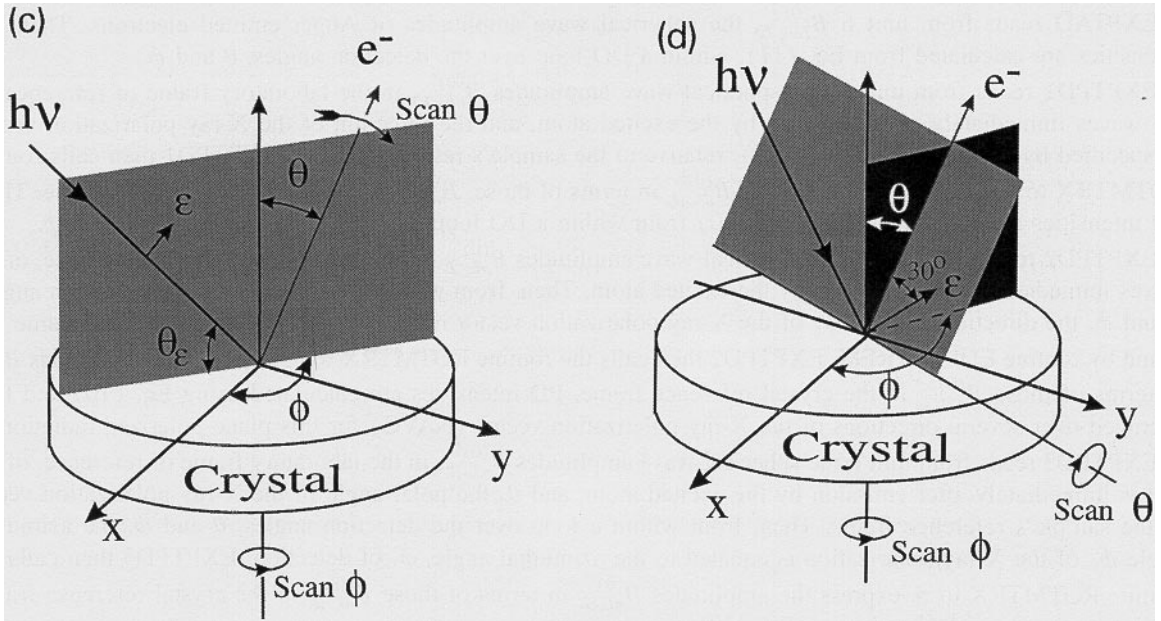


Fig. 1 — continued.

5. Overview of PAD programs

Angle-revolved Auger- and photoelectron diffraction intensities may be simulated with our suite of PAD programs, by running PAD1, PAD2, and PAD3 in sequence as shown in the flow chart of Fig. 1 of paper I of this set. The sequence is important, for PAD2 and PAD3 may be correctly compiled only after PAD1 is executed. This is due to the fact that an include file generated by PAD1 determines the sizes of arrays in the PAD2 and PAD3 programs, depending on the details of the calculation to be attempted.

In summary, PAD1 sets up a concentric-shell cluster and control parameters, PAD2 calculates the cluster transmission matrix, and PAD3 calculates the angle-resolved Auger- and photoelectron diffraction patterns for a choice of type of experiment.

6. Program structure of PAD3

In the current program package, four types of PD experiments may be modelled by the code. The switch between those experiment types is controlled by the parameter, NGEO:

- (1) NGEO=0, AD0 mode for Auger electron diffraction (geometry independent);
- (2) NGEO=1, PD1 mode, as shown in Fig. 1a;
- (3) NGEO=2, PD2 mode, a typical ESCA lab geometry, as shown in Fig. 1b;
- (4) NGEO=3, PD3 mode, as shown in Fig. 1c;
- (5) NGEO=4, PD4 mode, as shown in Fig. 1d.

The main program of PAD3 calls the subroutine READZ to get the distance of cluster below the surface from FORTRAN unit 4, and then calls READTOT to read in the elements of the cluster transmission matrix from unit 6. The main program then calls routines EXPTAD, EXPTPD1, EXPTPD2, EXPTPD3, or EXPTPD4 depending on the value of the parameter, NGEO.

EXPTAD reads from unit 6 $B_{\text{Aug},L}^{(0)}$, the spherical wave amplitudes of Auger emitted electrons. Then AD intensities are calculated from Eq. (11), within a DO loop over the detection angles, θ and ϕ .

EXPTPD1 reads from unit 6, the spherical-wave amplitudes $B_{nL_c,L}^{(0)'}$, in the laboratory frame of reference, of the waves immediately after emission by the excited atom, and the direction of the X-ray polarization vector, as specified by the polar angles (θ_e, ϕ_e) , relative to the sample's reference frame. EXPTPD1 then calls routine ROTMTRX to re-express the amplitudes $B_{nL_c,L}^{(0)'}$ in terms of those, $B_{nL_c,L}^{(0)}$ in the sample's reference frame. Then, PD intensities are calculated using Eq. (10) from within a DO loop over the detection angles, θ and ϕ .

EXPTPD2 reads from unit 6 the spherical-wave amplitudes $B_{nL_c,L}^{(0)'}$, in the laboratory frame of reference, of the waves immediately after emission by the excited atom. Then, from within a DO loop over the detection angles, θ and ϕ , the directions θ_e and ϕ_e of the X-ray polarization vector relative to the sample's reference frame, are found by routine EULERTRFM. EXPTPD2 then calls the routine ROTMTRX to re-express the amplitudes $B_L^{(0)'}$ in terms of those $B_{nL_c,L}^{(0)}$ in the crystal reference frame. PD intensities are calculated using Eq. (10) and then averaged over several directions of the X-ray polarization vector (NAVG) for this plane-polarized radiation.

EXPTPD3 reads from unit 6 the spherical-wave amplitudes $B_{nL_c,L}^{(0)'}$, in the laboratory frame of reference, of the waves immediately after emission by the excited atom, and θ_e the polar angle of the X-ray polarization vector in the sample's reference frame. Then, from within a loop over the detection angles, θ and ϕ , the azimuthal angle ϕ_e of the X-ray polarization is equated to the azimuthal angle, ϕ , of detection. EXPTPD3 then calls the routine ROTMTRX to re-express the amplitudes $B_{nL_c,L}^{(0)'}$ in terms of those $B_{nL_c,L}^{(0)}$ in the crystal reference frame. PD intensities are calculated using Eq. (10).

EXPTPD4 reads from unit 6 the spherical-wave amplitudes $B_{nL_c,L}^{(0)'}$, in the laboratory frame of reference, of the waves immediately after emission by the excited atom, Then, from within a loop over the detection angles, θ and ϕ , the directions θ_e and ϕ_e of the X-ray polarization vector are calculated by the routine EULERTRFM. EXPTPD4 calls ROTMTRX to re-express these amplitudes in terms of those $B_{nL_c,L}^{(0)}$ in the crystal reference frame. PD intensities are calculated using Eq. (10).

7. Input and output

The input and include files of PAD3 are generated automatically by PAD1 and PAD2. PAD3 outputs the simulated PD pattern on FORTRAN unit 9.

8. Test run

The test run from the supplied input data file calculates core-level O-1s PD, for an electron kinetic energy of 60 eV, for experiment type of PD3, illustrated in Fig. 1c of paper III of this set of papers. The O atom is assumed to occupy the 4-fold hollow site on a Ni(001) surface. In this run the full multiple-scattering option (IFWD=0) is assumed.

9. Other sample output

In addition to the output from the above test run, angle-resolved O-1s PD patterns from the same system, and the same electron kinetic energy, from the four experimental configurations, PD1, PD2, PD3, and PD4, are plotted as stereographic projections in Figs. 2a-d, respectively. The patterns are displayed in such a way that their centers mark the projection of the surface normal, and the edges of the patterns correspond to the polar

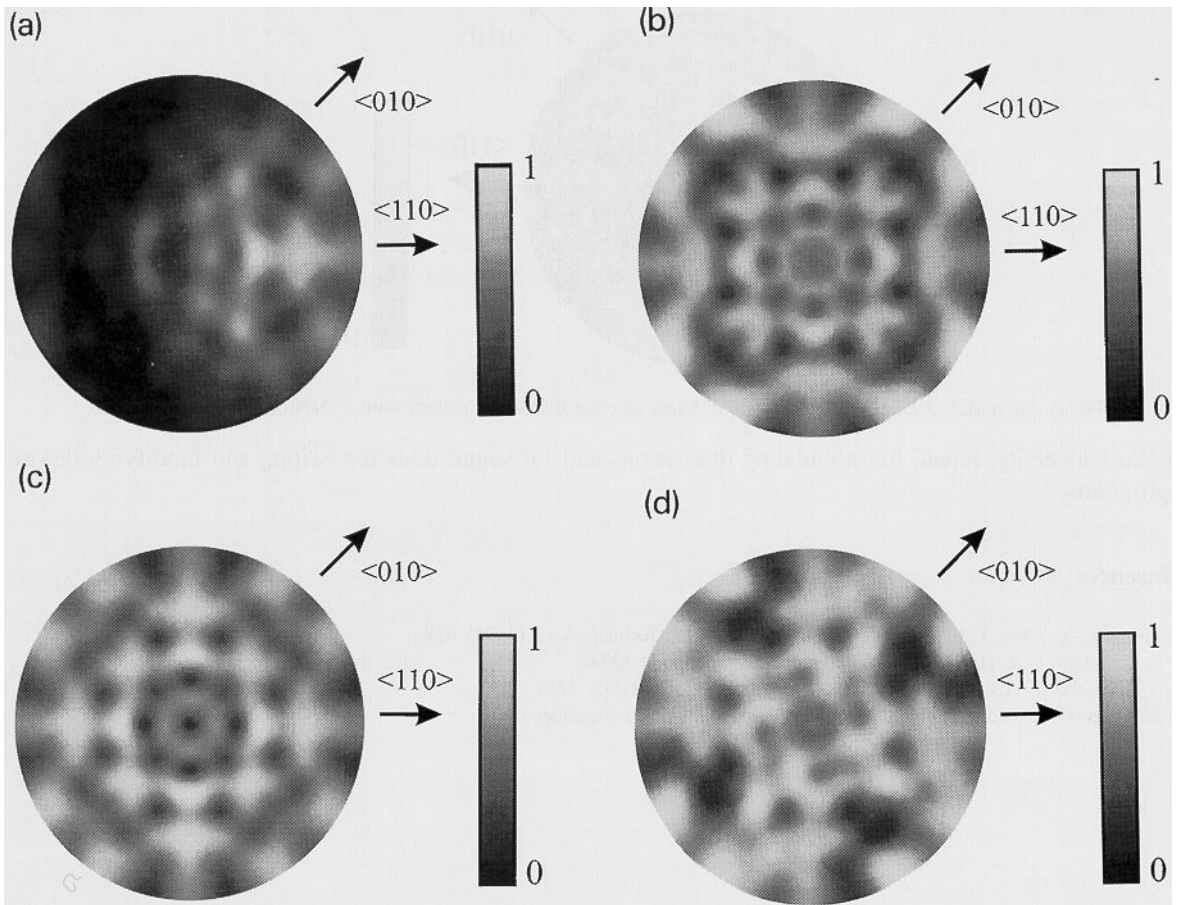


Fig. 2. (a) Simulated O-1s photoelectron diffraction pattern from an O/Ni(001)-p(2x2) surface, and the experimental geometry PD1 ($\theta_e = 45^\circ$, $\phi_e = 0^\circ$), illustrated in Fig. 1a.
 (b) Same as (a), except from the experimental geometry PD2, illustrated in Fig. 1b.
 (c) Same as (a), except from the experimental geometry PD3 ($\theta_e = 45^\circ$), shown in Fig. 1c.
 (d) Same as (a), except from the experimental geometry PD4, as illustrated in Fig. 1d. Note that, in this geometry, the symmetry of the diffraction pattern differs from that of the sample.

angle of detection, $\theta = 85^\circ$. It is apparent that the diffraction patterns expected from these different experimental geometries vary significantly for this low electron kinetic energy (60 eV).

For comparison, we show in Fig. 3 a simulated O $KL_{23}L_{23}$ Auger diffraction pattern (for an electron kinetic energy of 504 eV) for the same hollow site adsorption on a Ni(001) surface of the O atom. In this case, the outward-scattering (OS) approximation was assumed (IFWD=1), and the scattering cluster included all atoms at distances up to 15 Å from the emitter.

Acknowledgements

D.K.S. acknowledges support for this work from the National Science Foundation (Grant No. DMR-9320275) and from the Donors of the Petroleum Research Fund, administered by the American Chemical Society. The authors are grateful to Drs. S. Kono and T. Abukawa of the Research Institute for Scientific Measurements,

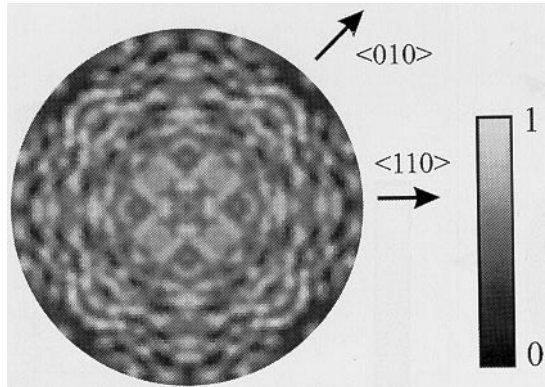


Fig. 3. Simulated O $KL_{23}L_{23}$ angle-resolved Auger electron diffraction pattern from a O/Ni(001)-p(2x2) surface.

Tohoku University, Japan, for stimulating discussions and for suggestions for writing and modifying this suite of programs.

References

- [1] See, e.g., X. Chen, G.R. Harp, D.K. Saldin, J. Vac. Sci. Technol. A 12 (1994) 428.
- [2] D.K. Saldin, G.R. Harp, X. Chen, Phys. Rev. B 48 (1993) 8234.
- [3] V. Fritzsche, J. Phys. Condens. Matter 2 (1990) 1413; 2 (1990) 9735.
- [4] X. Chen, D.K. Saldin, Comput. Phys. Commun. 112 (1998) 67, paper I.

TEST RUN OUTPUT

pattern.dat: Output file from pad3.f (stream 9)
(Only first 3 pages of this file are appended here)

Theta,Phi,Intensity
90 0 0.110E+00
90 1 0.109E+00
90 2 0.108E+00
90 3 0.105E+00
90 4 0.102E+00
90 5 0.985E-01
90 6 0.946E-01
90 7 0.905E-01
90 8 0.866E-01
90 9 0.830E-01
90 10 0.799E-01
90 11 0.774E-01
90 12 0.757E-01
90 13 0.748E-01
90 14 0.747E-01
90 15 0.754E-01
90 16 0.768E-01
90 17 0.789E-01
90 18 0.816E-01
90 19 0.848E-01
90 20 0.885E-01
90 21 0.925E-01
90 22 0.969E-01
90 23 0.101E+00
90 24 0.106E+00
90 25 0.111E+00
90 26 0.116E+00
90 27 0.120E+00
90 28 0.124E+00
90 29 0.127E+00
90 30 0.130E+00
90 31 0.131E+00
90 32 0.132E+00
90 33 0.131E+00
90 34 0.130E+00
90 35 0.127E+00
90 36 0.123E+00
90 37 0.119E+00
90 38 0.115E+00
90 39 0.110E+00
90 40 0.106E+00
90 41 0.102E+00
90 42 0.990E-01
90 43 0.965E-01
90 44 0.950E-01
90 45 0.945E-01
90 46 0.950E-01
90 47 0.965E-01
90 48 0.990E-01
90 49 0.102E+00
90 50 0.106E+00

90 51 0.110E+00
90 52 0.115E+00
90 53 0.119E+00
90 54 0.123E+00
90 55 0.127E+00
90 56 0.130E+00
90 57 0.131E+00
90 58 0.132E+00
90 59 0.131E+00
90 60 0.130E+00
90 61 0.127E+00
90 62 0.124E+00
90 63 0.120E+00
90 64 0.116E+00
90 65 0.111E+00
90 66 0.106E+00
90 67 0.101E+00
90 68 0.969E-01
90 69 0.925E-01
90 70 0.885E-01
90 71 0.848E-01
90 72 0.816E-01
90 73 0.789E-01
90 74 0.768E-01
90 75 0.754E-01
90 76 0.747E-01
90 77 0.748E-01
90 78 0.757E-01
90 79 0.774E-01
90 80 0.799E-01
90 81 0.830E-01
90 82 0.866E-01
90 83 0.905E-01
90 84 0.946E-01
90 85 0.985E-01
90 86 0.102E+00
90 87 0.105E+00
90 88 0.108E+00
90 89 0.109E+00
90 90 0.110E+00
90 91 0.109E+00
90 92 0.108E+00
90 93 0.105E+00
90 94 0.102E+00
90 95 0.985E-01
90 96 0.946E-01
90 97 0.905E-01
90 98 0.866E-01
90 99 0.830E-01
90 100 0.799E-01
90 101 0.774E-01
90 102 0.757E-01
90 103 0.748E-01
90 104 0.747E-01
90 105 0.754E-01
90 106 0.768E-01
90 107 0.789E-01

90 108 0.816E-01
90 109 0.848E-01
90 110 0.885E-01
90 111 0.925E-01
90 112 0.969E-01
90 113 0.101E+00
90 114 0.106E+00
90 115 0.111E+00
90 116 0.116E+00
90 117 0.120E+00
90 118 0.124E+00
90 119 0.127E+00
90 120 0.130E+00
90 121 0.131E+00
90 122 0.132E+00
90 123 0.131E+00
90 124 0.130E+00
90 125 0.127E+00
90 126 0.123E+00
90 127 0.119E+00
90 128 0.115E+00
90 129 0.110E+00
90 130 0.106E+00
90 131 0.102E+00
90 132 0.990E-01
90 133 0.965E-01
90 134 0.950E-01
90 135 0.945E-01
90 136 0.950E-01
90 137 0.965E-01
90 138 0.990E-01
90 139 0.102E+00
90 140 0.106E+00
90 141 0.110E+00
90 142 0.115E+00
90 143 0.119E+00
90 144 0.123E+00
90 145 0.127E+00
90 146 0.130E+00
90 147 0.131E+00
90 148 0.132E+00
90 149 0.131E+00
90 150 0.130E+00
90 151 0.127E+00
90 152 0.124E+00
90 153 0.120E+00
90 154 0.116E+00
90 155 0.111E+00
90 156 0.106E+00
90 157 0.101E+00
90 158 0.969E-01
90 159 0.925E-01
90 160 0.885E-01
90 161 0.848E-01
90 162 0.816E-01
90 163 0.789E-01
90 164 0.768E-01